EUROPEAN ORGANIZATION FOR NUCLEAR RESEARCH

European Organization for Particle Physics

Analysing the FMD data for $\frac{1}{N}\frac{dN_{\mathbf{ch}}}{d\eta}$

ALICE–INT–2012–040 v2
July 12, 2012

Christian Holm Christensen* & Hans Hjersing Dalsgaard†
Niels Bohr Institute
University of Copenhagen

Contents

*⟨cholm@nbi.dk⟩
†⟨canute@nbi.dk⟩

1 Introduction

This document describes the steps performed in the analysis of the charged particle multiplicity in the forward pseudo–rapidity regions with the FMD detector [1, 2]. The document also include a summary (see section 7) of the request for preliminary figures for the measurement of $\frac{1}{N}\frac{dN_{\mathrm{ch}}}{d\eta}$ with SPD[7, 8], VZERO[3], and FMD.

The FMD is organised in 3 *sub–detectors* FMD1, FMD2, and FMD3, each consisting of 1 (FMD1) or 2 (FMD2 and 3) *rings*. The rings fall into two types: *Inner* or *outer* rings. Each ring is in turn azimuthally divided into *sectors*, and each sector is radially divided into *strips*. How many sectors, strips, as well as the η coverage is given in Table 1.

Table 1: Physical dimensions of Si segments and strips.

Sub–detector/ Ring	**Azimuthal sectors**	**Radial strips**	z **[cm]**	r **range [cm]**	η **coverage**
FMD1i	20	512	320	4.2 – 17.2	3.68 – 5.03
FMD2i	20	512	83.4	4.2 – 17.2	2.28 – 3.68
FMD2o	40	256	75.2	15.4 – 28.4	1.70 – 2.29
FMD3i	20	512	-75.2	4.2 – 17.2	-2.29 – -1.70
FMD3o	40	256	-83.4	15.4 – 28.4	-3.40 – -2.01

The FMD ESD object contains the scaled energy deposited $\Delta E/\Delta E_{mip}$ for each of the 51,200 strips. This is determined in the reconstruction pass. The scaling to ΔE_{mip} is done using calibration factors extracted in designated pulser runs. In these runs, the front-end electronics is pulsed with an increasing known pulse size, and the conversion factor from ADC counts to ΔE_{mip} is determined [2].

The SPD is used for determination of the position of the primary interaction point except in the case of displaced vertex analysis as discussed in section 2.1.1.

The analysis is performed as a two–step process.

1. The Event–Summary–Data (ESD) is processed event–by–event and passed through a number of algorithms, and $\frac{d^2N_{\mathrm{ch}}}{d\eta\,d\varphi}$ for each event is output to an Analysis–Object–Data (AOD) tree (see Section 2).
2. The AOD data is read in and the sub–sample of the data under investigation is selected (e.g., INEL, INEL > 0, NSD in p+p data, or some centrality class in Pb+Pb data) and the $\frac{d^2N_{\mathrm{ch}}}{d\eta\,d\varphi}$ histogram read for those events to build up $\frac{1}{N}\frac{dN_{\mathrm{ch}}}{d\eta}$ (see Section 3).

The details of each step above will be expanded upon in the following.

In Appendix A is an overview of the nomenclature used in this document.

2 Generating $\left.\frac{d^2N_{\mathrm{ch}}}{d\eta\,d\varphi}\right|_i$ event–by–event

When reading in the ESDs and generating the $\frac{d^2N_{\mathrm{ch}}}{d\eta\,d\varphi}$ event–by–event the following steps are taken (in order) for each event i and FMD ring r.

Event inspection The global properties of the event is determined, including the trigger type and primary interaction point[1] z coordinate (see Section 2.1).

Sharing filter The ESD object is read in and corrected for sharing. The result is a new ESD object (see Section 2.2).

Density calculator The (possibly un–corrected) ESD object is then inspected and an inclusive (primary *and* secondary particles), per–ring charged particle density $\left.\frac{d^2N_{\mathrm{ch}}}{d\eta\,d\varphi}\right|_{incl,r,v,i}$ is made. This calculation depends in general upon the interaction vertex position along the z axis v_z (see Section 2.3).

Corrections The 5 (one for each FMD ring) $\left.\frac{d^2N_{\mathrm{ch}}}{d\eta\,d\varphi}\right|_{incl,r,v,i}$ are corrected for secondary production and acceptance. The correction for the secondary particle production is highly dependent on the vertex z coordinate. The result is a per–ring, charged primary particle density $\left.\frac{d^2N_{\mathrm{ch}}}{d\eta\,d\varphi}\right|_{r,v,i}$ (see Section 2.4).

Histogram collector Finally, the 5 $\left.\frac{d^2N_{\mathrm{ch}}}{d\eta\,d\varphi}\right|_{r,v,i}$ are summed into a single $\left.\frac{d^2N_{\mathrm{ch}}}{d\eta\,d\varphi}\right|_{v,i}$ histogram, taking care of the overlaps between the detector rings. In principle, this histogram is independent of the vertex, except that the pseudo–rapidity range, and possible holes in that range, depends on v_z — or rather the bin in which the v_z falls (see Section 2.5).

Each of these steps will be detailed in the following.

2.1 Event inspection

The first thing to do, is to inspect the event for triggers. A number of trigger bits, like INEL (Minimum Bias for Pb+Pb), INEL > 0, NSD, and so on is then propagated to the AOD output.

Just after the sharing filter (described below) but before any further processing, the vertex information is queried. If there is no vertex information, or if the vertex z coordinate is outside the pre–defined range, then no further processing of that event takes place.

2.1.1 Displaced Vertices

The analysis can be set up to run on the 'displaced vertices' that occur during LHC Pb+Pb running. Details on the displaced vertices, and their selection can be found in the VZERO analysis note [3].

[1] 'Vertex' and 'primary interaction point' will be used interchangeably in the text, since there is no ambiguity with particle production vertex in this analysis.

2.2 Sharing filter

A particle originating from the vertex can, because of its incident angle on the FMD sensors traverse more than one strip (see Figure 1). This means that the energy loss of the particle is distributed over 1 or more strips. The signal in each strip should therefore possibly be merged with its neighboring strip signals to properly reconstruct the energy loss of a single particle.

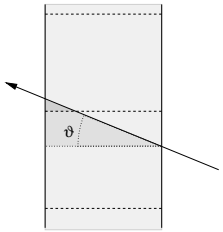

Figure 1: A particle traversing 2 strips and depositing energy in each strip.

The effect is most pronounced in low–flux[2] events, like proton–proton collisions or peripheral Pb–Pb collisions, while in high–flux events the hit density is so high that most likely each and every strip will be hit and the effect cancels out on average.

Since the particles travel more or less in straight lines toward the FMD sensors, the sharing effect is predominantly in the r or *strip* direction. Only neighbouring strips in a given sector are therefore investigated for this effect.

Algorithm 1 is applied to the signals in a given sector.

Algorithm 1: Sharing correction

```
1  current strip used ← false;
2  previous strip used ← false;
3  for t ← 1 to # strips do
4      output_t ← 0;
5      current ← SignalInStrip (t);
6      if current is not valid then
7          output_t ← invalid;
8      else if current is 0 then
9          output_t ← 0;
10     else
11         η ← η of input_t;
12         previous strip signal ← 0;
13         next strip signal ← 0;
14         if t ≠ 1 then previous strip signal ← SignalInStrip (t − 1);
15         if t ≠# strips then next strip signal ← SignalInStrip (t + 1);
16         output_t ← MultiplicityOfStrip (current,η,previous strip signal,next strip signal,
17                                         low flux flag,t,previous strip used,current strip used);
```

Here the function `SignalInStrip`(t) returns the properly path–length corrected signal in strip t. The function `MultiplicityOfStrip` is where the real processing takes place (see page 5).

Here, the function `GetHighCut` (see below) evaluates a fit to the energy distribution in the specified η bin (see also Section 2.3). It returns

$$\Delta_{mp} - 2w$$

where Δ_{mp} is the most probable energy loss, and w is the width of the Landau distribution.

[2] Events with a low hit density.

Function `MultiplicityOfStrip` (current, η, previous, next, low flux flag, previous signal used, this signal used)

```
1  if current is very large or current < low cut then
2      this signal used ← false;
3      previous signal used ← false;
4      return 0
5  if this signal used then
6      this signal used ← false;
7      previous signal used ← true;
8      return 0
9  high cut ← GetHighCut (t,η);
10 Total ← current;
11 if low cut < previous < high cut and not previous signal used then Total ← Total + previous;
12 if low cut < next < high cut then
13     Total ← Total + next;
14     this signal used ← true;
15 if Total > 0 then
16     previous signal used ← true;
17     return Total
18 else
19     previous signal used ← false;
20     this signal used ← false;
21     return 0
```

The **if** in line 5, says that if the previous strip was merged with current one, and the signal of the current strip was added to that, then the current signal is set to 0, and we mark it as used for the next iteration (previous signal used←true).

In line 11, we test if the previous signal lies between our low and high cuts, and if it has not been marked as being used. If so, we add it to our current signal.

The next **if** on line 12 checks if the next signal is within our cut bounds. If so, we add that signal to the current signal and mark it as used for the next iteration (this signal used←true). It will then be put to zero on the next iteration by the condition on line 6.

Finally, if our signal is still larger than 0, we return the signal and mark this signal as used (previous signal used←true) so that it will not be used in the next iteration. Otherwise, we mark the current signal and the next signal as unused and return a 0.

2.3 Density calculator

The density calculator loops over all the strip signals in the sharing corrected[3] ESD and calculates the inclusive (primary + secondary) charged particle density in pre–defined (η, φ) bins.

[3]The sharing correction can be disabled, in which case the density calculator uses the input ESD signals.

2.3.1 Inclusive number of charged particles: Energy Fits

The number charged particles in a strip $N_{\mathrm{ch},t}$ is calculated using multiple Landau-like distributions fitted to the energy loss spectrum of all strips in a given η bin.

$$\begin{aligned}
\Delta_{i,mp} &= i(\Delta_{1,mp} + \xi_1 \log(i)) \\
\xi_i &= i\xi_1 \\
\sigma_i &= \sqrt{i}\sigma_1 \\
N_{\mathrm{ch},t} &= \frac{\sum_i^{N_{max}} i\, a_i F(\Delta_t; \Delta_{i,mp}, \xi_i, \sigma_i)}{\sum_i^{N_{max}} a_i F(\Delta_t; \Delta_{i,mp}, \xi_i, \sigma_i)} \quad ,
\end{aligned} \tag{1}$$

where $F(x;\Delta_{mp},\xi,\sigma)$ is the evaluation of the Landau distribution f_L with most probable value Δ_{mp} and width ξ, folded with a Gaussian distribution with spread σ at the energy loss x [4, 5].

$$F(x;\Delta_{mp},\xi,\sigma) = \frac{1}{\sigma\sqrt{2\pi}} \int_{-\infty}^{+\infty} d\Delta' f_L(x;\Delta',\xi) \exp -\frac{(\Delta_{mp}-\Delta')^2}{2\sigma^2} \quad , \tag{2}$$

where $\Delta_{1,mp}$, ξ_1, and σ_1 are the parameters for the first MIP peak, $a_1 = 1$, and a_i is the relative weight of the i-fold MIP peak. The parameters $\Delta_{1,mp}, \xi_1, \sigma_1, \mathbf{a} = (a_2, \ldots a_{N_{max}})$ are obtained by fitting

$$F_j(x;C,\Delta_{mp},\xi,\sigma,\mathbf{a}) = C\sum_{i=1}^{j} a_i F(x;\Delta_{i,mp},\xi_i,\sigma_i)$$

for increasing j to the energy loss spectra in separate η bins. The fit procedure is stopped when for $j+1$: (the default values for each value are included below)

- the reduced χ^2 exceeds a certain threshold (usually 20), or
- the relative error $\delta p/p$ of any parameter of the fit exceeds a certain threshold (usually 0.12), or
- when the weight $a_j + 1$ is smaller than some number (typically 10^{-5}).

N_{max} is then set to j. Examples of the result of these fits are given in Figure 18 in Appendix C.

2.3.2 Inclusive number of charged particles: Poisson Approach

Another approach to the calculation of the number of charged particles is using Poisson statistics. This is the default choice because it is less sensitive to the stability of the fits required for the energy fits method. Assume that in a region of the FMD N_{ch} is distributed according to a Poisson distribution. This means that the probability of $N_{\mathrm{ch}} = n$ becomes:

$$P(n) = \frac{\mu^n e^{-\mu}}{n!} \tag{3}$$

In particular the measured occupancy, μ_{meas}, is the probability of any number of hits, thus using (3) :

$$\mu_{meas} = 1 - P(0) = 1 - e^{-\mu} \tag{4}$$

which implies:

$$\mu = \ln(1-\mu_{meas})^{-1} \tag{5}$$

The mean number of particles in a hit strip becomes:

$$\begin{aligned}
C &= \frac{\sum_{n>0} nP(n>0)}{\sum_{n>0} P(n>0)} \\
&= \frac{e^{-\mu}}{1-e^{-\mu}} \mu \sum \frac{\mu^n}{n!} \\
&= \frac{e^{-\mu}}{1-e^{-\mu}} \mu e^{\mu} \\
&= \frac{\mu}{1-e^{-\mu}}
\end{aligned} \tag{6}$$

With μ defined in (5) this calculation is carried out per event in regions of the FMD each containing 256 strips[4]. In such a region, N_{ch} for a hit strip ($N_{hits} \equiv 1$) in that region becomes:

$$N_{\mathrm{ch}} = N_{hits} \times C = 1 \times C = C \tag{7}$$

Where C is calculated using μ_{meas}^{region}.

The Poisson method and the energy fits method have been compared in [6] where it is found that the two methods are in good agreement. The residual difference between the methods contributes to the systematic error.

2.3.3 Azimuthal Acceptance

Before the signal $N_{\mathrm{ch},t}$ can be added to the (η, φ) bin in one of the 5 per–ring histograms, it needs to be corrected for the φ acceptance of the strip.

The sensors of the FMD are not perfect arc–segments — the two top corners are cut off to allow the largest possible sensor on a 6" Si-wafer. This means, however, that the strips in these outer regions do not fully cover 2π in azimuth, and there is therefore a need to correct for this limited acceptance.

The acceptance correction is only applicable where the strip length does not cover the full sector. This is the case for the outer strips in both the inner and outer type rings. The acceptance correction is then simply

$$A_t^{\varphi} = \frac{l_t}{\Delta\varphi} \tag{8}$$

where l_t is the strip length in radians at constant r, and $\Delta\varphi$ is 2π divided by the number of sectors in the ring (20 for inner type rings, and 40 for outer type rings).

Note, that this correction is a hardware–related correction, and does not depend on the properties of the collision (e.g., primary vertex location).

The final (η, φ) content of the 5 output vertex dependent, per–ring histograms of the inclusive charged particle density is then given by

$$\left.\frac{d^2N_{\mathrm{ch}}}{d\eta\, d\varphi}\right|_{incl,r,v,i(\eta,\varphi)} = \sum_{t}^{t\in(\eta,\varphi)} N_{\mathrm{ch},t} A_t^{\varphi} \tag{9}$$

where t runs over the strips in the (η, φ) bin.

2.4 Corrections

The corrections code receives the five vertex dependent, per–ring histograms of the inclusive charged particle density $\left.\frac{d^2N_{\mathrm{ch}}}{d\eta\, d\varphi}\right|_{incl,r,v,i}$ from the density calculator and applies two corrections

2.4.1 Secondary correction

This is a 2 dimensional histogram generated from simulations, as the ratio of primary particles to the total number of particles that fall within an (η, φ) bin for a given vertex bin

$$S_v(\eta,\varphi) = \frac{\sum_i^{N_{\mathrm{V},v}} N_{\mathrm{ch,primary},i}(\eta,\varphi)}{\sum_i^{N_{\mathrm{V},v}} N_{\mathrm{ch,FMD},i}(\eta,\varphi)} \quad , \tag{10}$$

[4] Note that this means that the same factor is used for each of the 256 strips.

where $N_{\mathrm{V},v}$ is the number of events with a valid trigger and a vertex in bin v, and $N_{\mathrm{ch,FMD},i}$ is the total number of charged particles that hit the FMD in event i in the specified (η,φ) bin and $N_{\mathrm{ch,primary},i}$ is number of primary charged particles in event i within the specified (η,φ) bin.

$N_{\mathrm{ch,primary}}(\eta,\varphi)$ is given by summing over the charged particles labelled as primaries *at the time of the collision* as defined in the simulation code. That is, it is the number of primaries within the (η,φ) bin at the collision point — not at the FMD.

$S_v(\eta,\varphi)$ varies from ≈ 1.5 for the most forward bins to ≈ 3 for the more central bins. Figure 2 shows the $\frac{1}{N}\frac{dN_{\mathrm{ch}}}{d\eta}$ of secondaries from various sources assessed with MC simulations to give an idea of the magnitude of the effects of secondaries.

For pp, at least some millions of events must be accumulated to reach satisfactory statistics. For Pb–Pb where the general hit density is larger, reasonable statistics can be achieved with less simulated data.

2.4.2 Acceptance due to dead channels

Some of the strips in the FMD have been marked up as *dead*, meaning that they are not used in the reconstruction or analysis. This leaves holes in the acceptance of each defined (η,φ) which need to be corrected for.

Dead channels are marked specially in the ESDs with the flag *Invalid Multiplicity*. This is used in the analysis to build up and event–by–event acceptance correction in each (η,φ) bin by calculating the ratio

$$A^{\eta}_{v,i}(\eta,\varphi) = \frac{\sum_t^{t\in(\eta,\varphi)} \begin{cases} 1 & \text{if not dead} \\ 0 & \text{otherwise} \end{cases}}{\sum_t^{t\in(\eta,\varphi)} 1} \quad , \tag{11}$$

where t runs over the strips in the (η,φ) bin. This correction is obviously v_z dependent since the (η,φ) bin to which a strip t corresponds to depends on its position relative to the primary vertex.

Alternatively, pre–made acceptance factors can be used. These are made from the off-line conditions database (OCDB).

The 5 output vertex dependent, per–ring histograms of the primary charged particle density is then given by

$$\left.\frac{d^2N_{\mathrm{ch}}}{d\eta\,d\varphi}\right|_{r,v,i(\eta,\varphi)} = S_v(\eta,\varphi)\frac{1}{A^{\eta}_{v,i}(\eta,\varphi)}\left.\frac{d^2N_{\mathrm{ch}}}{d\eta\,d\varphi}\right|_{incl,r,v,i(\eta,\varphi)} \tag{12}$$

2.5 Histogram collector

The histogram collector collects the information from the 5 vertex dependent, per–ring histograms of the primary charged particle density $\left.\frac{d^2N_{\mathrm{ch}}}{d\eta\,d\varphi}\right|_{r,v,i}$ into a single vertex dependent histogram of the charged particle density $\left.\frac{d^2N_{\mathrm{ch}}}{d\eta\,d\varphi}\right|_{v,i}$.

To do this, it first calculates, for each vertex bin, the η bin range to use for each ring. It investigates the secondary correction maps $S_v(\eta,\varphi)$ to find the edges of each map. The edges are given by the η range where $S_v(\eta,\varphi)$ is larger than some threshold[5] t_s. The code applies safety margin of a number of bins, N_{cut}[6], to ensure that the data selected does not have too large corrections associated with it.

It then loops over the bins in the defined η range and sums the contributions from each of the 5 histograms. In the η ranges where two rings overlap, the collector calculates the average and adds the errors in quadrature[7].

[5] Typically $t_s \approx 0.1$.
[6] Typically $N_{cut} = 1$.
[7] While not explicitly checked, it was found that the histograms agrees within error bars in the overlapping region

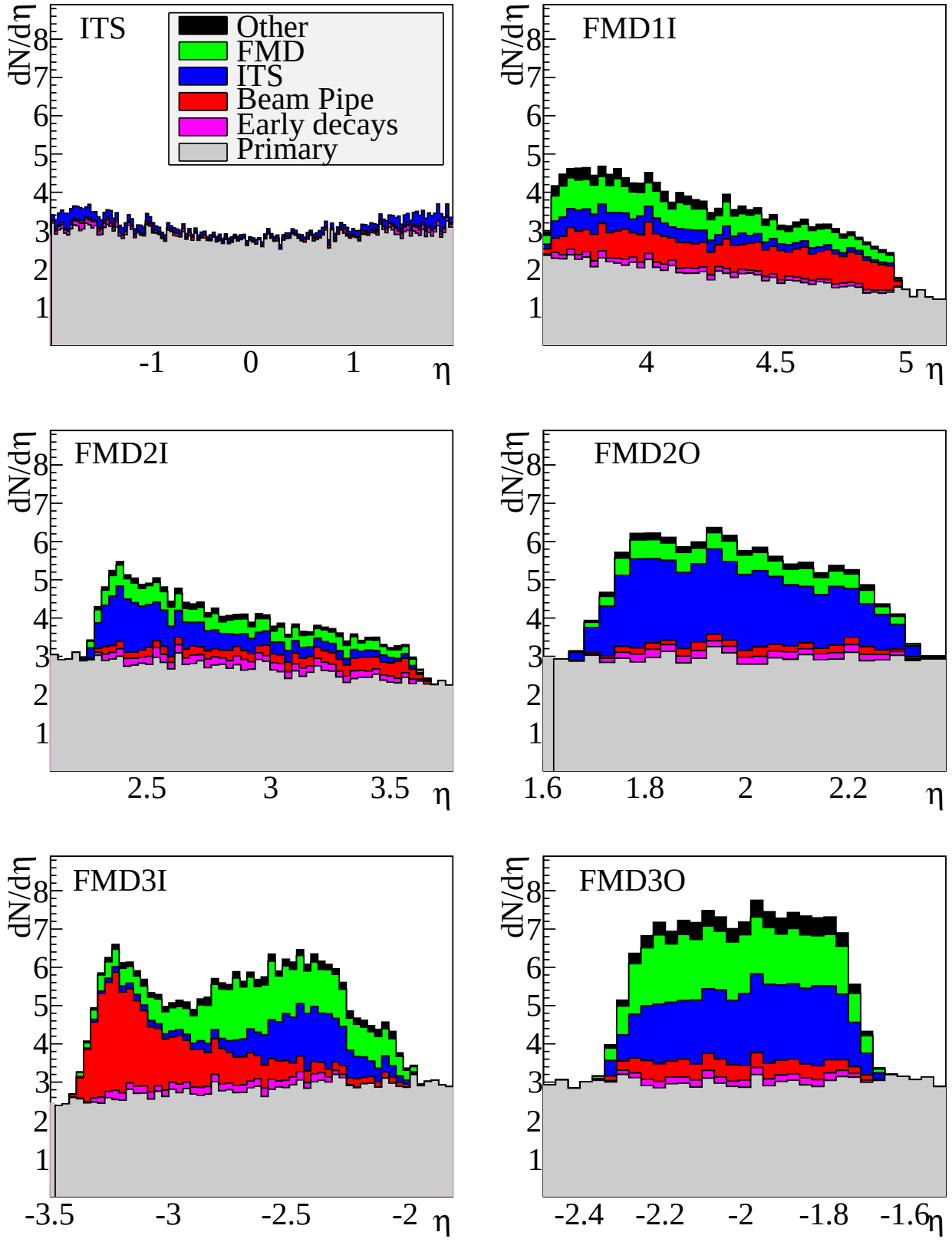

Figure 2: $\frac{1}{N}\frac{dN_{\mathrm{ch}}}{d\eta}$ for secondaries and primaries in the FMD. The same plot for the SPD inner layer is included for comparison.

The output vertex dependent histogram of the primary charged particle density is then given by

$$\left.\frac{d^2N_{\rm ch}}{d\eta\, d\varphi}\right|_{v,i(\eta,\varphi)} = \frac{1}{N_{r\in(\eta,\varphi)}} \sum_{r}^{r\in(\eta,\varphi)} \left.\frac{d^2N_{\rm ch}}{d\eta\, d\varphi}\right|_{r,v,i(\eta,\varphi)} \tag{13}$$

$$\delta\left[\left.\frac{d^2N_{\rm ch}}{d\eta\, d\varphi}\right|_{v,i(\eta,\varphi)}\right] = \frac{1}{N_{r\in(\eta,\varphi)}} \sqrt{\sum_{r}^{r\in(\eta,\varphi)} \delta\left[\left.\frac{d^2N_{\rm ch}}{d\eta\, d\varphi}\right|_{r,v,i(\eta,\varphi)}\right]^2} \quad , \tag{14}$$

where $N_{r\in(\eta,\varphi)}$ is the number of overlapping histograms in the given (η,φ) bin.

The histogram collector stores the found η ranges in the underflow bin of the histogram produced. The content of the overflow bins are

$$I_{v,i}(\eta) = \frac{1}{N_{r\in(\eta)}} \sum_{r}^{r\in(\eta)} \begin{cases} 0 & \eta \text{ bin not selected} \\ 1 & \eta \text{ bin selected} \end{cases} \quad , \tag{15}$$

where $N_{r\in(\eta)}$ is the number of overlapping histograms in the given η bin. The subscript v indicates that the content depends on the current vertex bin of event i.

3 Building the final $\frac{1}{N}\frac{dN_{\rm ch}}{d\eta}$

To build the final $\frac{1}{N}\frac{dN_{\rm ch}}{d\eta}$ distribution it is enough to sum (13) and (15) over all accepted events, $N_{\rm A}$, and correct for the acceptance $I(\eta)$

$$\left.\frac{d^2N_{\rm ch}}{d\eta\, d\varphi}\right|_{(\eta,\varphi)} = \sum_{i}^{N_{\rm A}} \left.\frac{d^2N_{\rm ch}}{d\eta\, d\varphi}\right|_{i,v(\eta,\varphi)} \tag{16}$$

$$I(\eta) = \sum_{i}^{N_{\rm A}} I_{i,v}(\eta) \quad . \tag{17}$$

Note, that $I(\eta) \leq N_{\rm A}$.

We then need to normalise to the total number of events N_X, given by

$$\begin{aligned} N_X &= \frac{1}{\varepsilon_X}\left[N_{\rm A} + \alpha(N_{\bar{\rm V}} - \beta)\right] \\ &= \frac{1}{\varepsilon_X}\left[N_{\rm A} + \frac{N_{\rm A}}{N_{\rm V}}(N_{\rm T} - N_{\rm V} - \beta)\right] \\ &= \frac{1}{\varepsilon_X} N_{\rm A}\left[1 + \frac{1}{\varepsilon_V} - 1 - \frac{\beta}{N_{\rm V}}\right] \\ &= \frac{1}{\varepsilon_X}\frac{1}{\varepsilon_V} N_{\rm A}\left(1 - \frac{\beta}{N_{\rm T}}\right) \end{aligned} \tag{18}$$

where

ε_X is the trigger efficiency for type $X \in [\text{INEL}, \text{INEL} > 0, \text{NSD} for p + p data and MB for Pb + Pb data]$

$\varepsilon_V = \frac{N_{\rm V}}{N_{\rm T}}$ is the vertex efficiency evaluated over the data.

$N_{\rm A}$ is the number of events with a trigger *and* a valid vertex in the selected range

$N_{\rm V}$ is the number of events with a trigger *and* a valid vertex.

$N_{\rm T}$ is the number of events with a trigger.

$N_{\bar{\rm V}} = N_{\rm T} - N_{\rm V}$ is the number of events with a trigger *but no* valid vertex

Effect	Magnitude in Pb+Pb analysis	Magnitude in p+p analysis
Variation of the cuts in sec. 2.2	2%	3%
Calculation of N_{ch}	3%	4%
Material budget	7 %	7 %
Generator	2%	2%
Vertex and trigger bias	N/A	3%
Centrality	1% –6%	N/A
Normalization	N/A	1.3% - 3%
Total in quadrature	8.2% – 10.1%	9.4 % – 9.8%

Table 2: The table summarizes the systematic errors in the FMD including the total systematic error obtained by addition in quadrature.

$\alpha = \frac{N_{\mathrm{A}}}{N_{\mathrm{V}}}$ is the fraction of accepted events of the total number of events with a trigger and valid vertex.

$\beta = N_a + N_c - N_e$ is the number of background events *with* a valid off-line trigger. This formula is the simplest case of one bunch crossing per trigger/background class. For more complicated collision setups the fractions in the formula change.

The two terms under the parenthesis in (18) refers to the observed number of event N_{A}, and the events missed because of no vertex reconstruction. Note, for $\beta \ll N_{\mathrm{T}}$ (18) reduces to the simpler expression

$$N_X = \frac{1}{\varepsilon_X}\frac{1}{\varepsilon_V}N_{\mathrm{A}}$$

The trigger efficiency ε_X for a given trigger type X is evaluated from simulations as

$$\varepsilon_X = \frac{N_{X\wedge \mathrm{T}}}{N_X} \quad , \tag{19}$$

that is, the ratio of number of events of type X with a corresponding trigger to the number of events of type X.

The final event–normalised charged particle density then becomes

$$\frac{1}{N}\frac{dN_{\mathrm{ch}}}{d\eta} = \frac{1}{N_X}\int_0^{2\pi} d\varphi \frac{\frac{d^2N_{\mathrm{ch}}}{d\eta\, d\varphi}\Big|_{(\eta,\varphi)}}{I(\eta)} \tag{20}$$

If the trigger X introduces a bias on the measured number of events, then (20) need to be modified to

$$\frac{1}{N}\frac{dN_{\mathrm{ch}}}{d\eta} = \frac{1}{N_X}\int_0^{2\pi} d\varphi \frac{\frac{1}{B(\eta,\varphi)}\frac{d^2N_{\mathrm{ch}}}{d\eta\, d\varphi}\Big|_{(\eta,\varphi)}}{I(\eta)} \quad , \tag{21}$$

where $B(\eta,\varphi)$ is the bias correction. This is typically calculated from simulations using the expression

$$B(\eta,\varphi) = \frac{\frac{1}{N_{X\wedge \mathrm{T}}}\sum_i^{N_{X\wedge \mathrm{T}}} N_{\mathrm{ch,primary}}(\eta,\varphi)}{\frac{1}{N_X}\sum_i^{N_X} N_{\mathrm{ch,primary}}(\eta,\varphi)} \tag{22}$$

4 Systematic Errors

The systematic errors on the $\frac{1}{N}\frac{dN_{\mathrm{ch}}}{d\eta}$ measurement are discussed in detail in [6]. The results for the systematic errors in p+p and Pb+Pb data are shown in table 2. A short summary of the elements of the table is given here:

- The variations of the cuts in section 2.2 are carried out by re–running the analysis with different cuts and taking the observed differences as the contribution to the systematic error.

- To assess the error on the calculation of the multiplcity the two methods for counting particles (see section 2.3) are compared.
- The systematic error on the material budget description was found from simulations with $\pm 10\%$ increased density.
- Several event generators were used to assess the error from the particular choice of generator in the analysis. The same procedure was used to assess the error from the MC dependent part of the correction for trigger and vertex bias (p+p only).
- The systematic error on the centrality selection was obtained from variations of the different methods for measuring centrality.

5 Using the per–event $\left.\frac{d^2N_{\mathrm{ch}}}{d\eta\, d\varphi}\right|_{i,v}$ histogram for other analysis

5.1 Multiplicity distribution

To build the multiplicity distribution for a given η range $[\eta_1, \eta_2]$, one needs to find the total multiplicity in that η range for each event. To do so, one should sum the $\left.\frac{d^2N_{\mathrm{ch}}}{d\eta\, d\varphi}\right|_{i,v}$ histogram over all φ and in the selected η range.

$$n'_{i[\eta_1,\eta_2]}, = \int_{\eta_1}^{\eta_2} d\eta \int_0^{2\pi} d\varphi \left.\frac{d^2N_{\mathrm{ch}}}{d\eta\, d\varphi}\right|_{i,v} \quad .$$

However, n'_i is not corrected for the coverage in η for the particular vertex range v. One therefor needs to correct for the number of missing bins in the range $[\eta_1, \eta_2]$. Suppose $[\eta_1, \eta_2]$ covers $N_{[\eta_1,\eta_2]}$ η bins, then the acceptance correction is given by

$$A_{i,[\eta_1,\eta_2]} = \frac{N_{[\eta_1,\eta_2]}}{\int_{\eta_1}^{\eta_2} d\eta\, I_{i,v}(\eta)} \quad .$$

The per–event multiplicity is then given by

$$\begin{aligned} n_{i,[\eta_1,\eta_2]} &= A_{i,[\eta_1,\eta_2]}\, n'_{i,[\eta_1,\eta_2]} \\ &= \frac{N_{[\eta_1,\eta_2]}}{\int_{\eta_1}^{\eta_2} \eta I_{i,v}(\eta)} \int_{\eta_1}^{\eta_2} d\eta \int_0^{2\pi} d\varphi \left.\frac{d^2N_{\mathrm{ch}}}{d\eta\, d\varphi}\right|_{i,v} \end{aligned} \tag{23}$$

5.2 Forward–Backward correlations

To do forward–backward correlations, one need to calculate $n_{i,[\eta_1,\eta_2]}$ as shown in (23) in two bins $n_{i,[\eta_1,\eta_2]}$ and $n_{i,[-\eta_2,-\eta_1]}$ *e.g.*, $n_{i,f} = n_{i,[-3,-1]}$ and $n_{i,b} = n_{i,[1,3]}$.

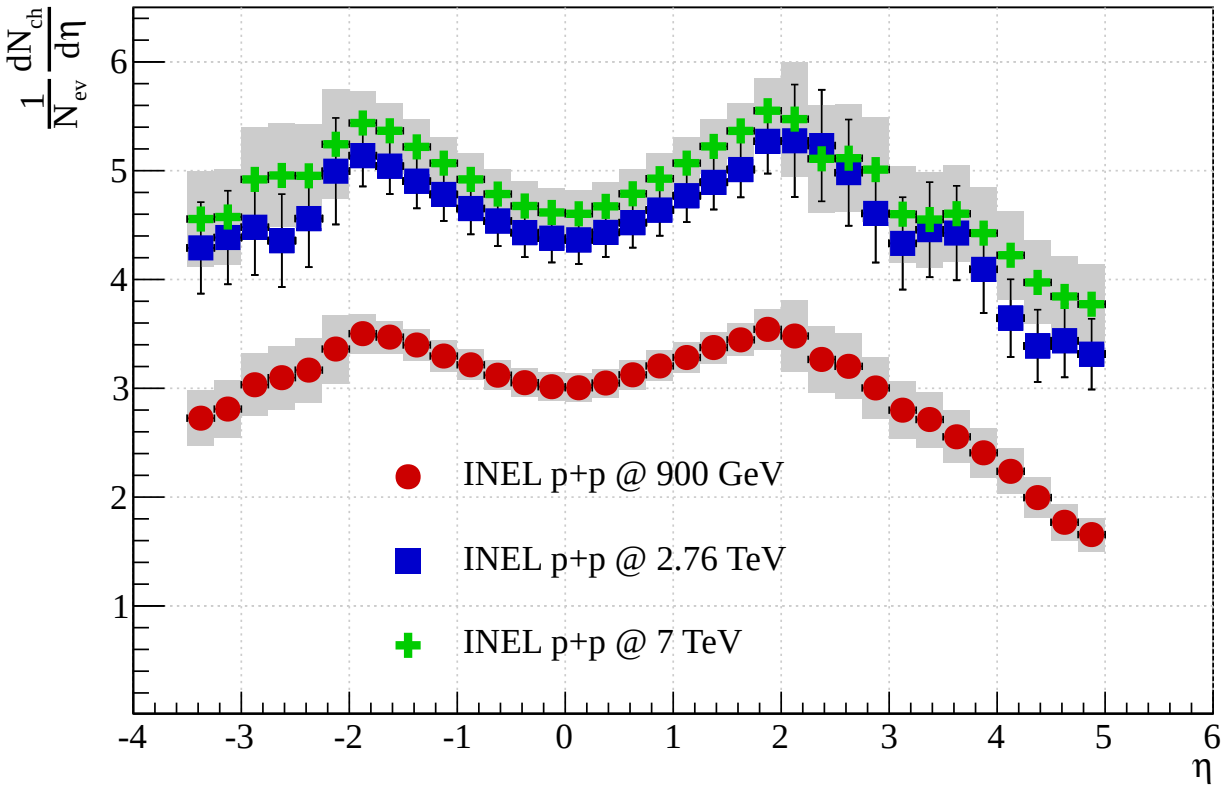

Figure 3: $\frac{1}{N}\frac{dN_{\rm ch}}{d\eta}$ for pp for INEL events at $\sqrt{s} = 900\,\text{GeV}$, $\sqrt{s} = 2.76\,\text{TeV}$, and $\sqrt{s} = 7\,\text{TeV}$ $-10\,\text{cm} \leq v_z \leq 10\,\text{cm}$, rebinned by a factor 5 [6].

6 Some results

Figures below show some examples [6]. Note these are not finalised plots.

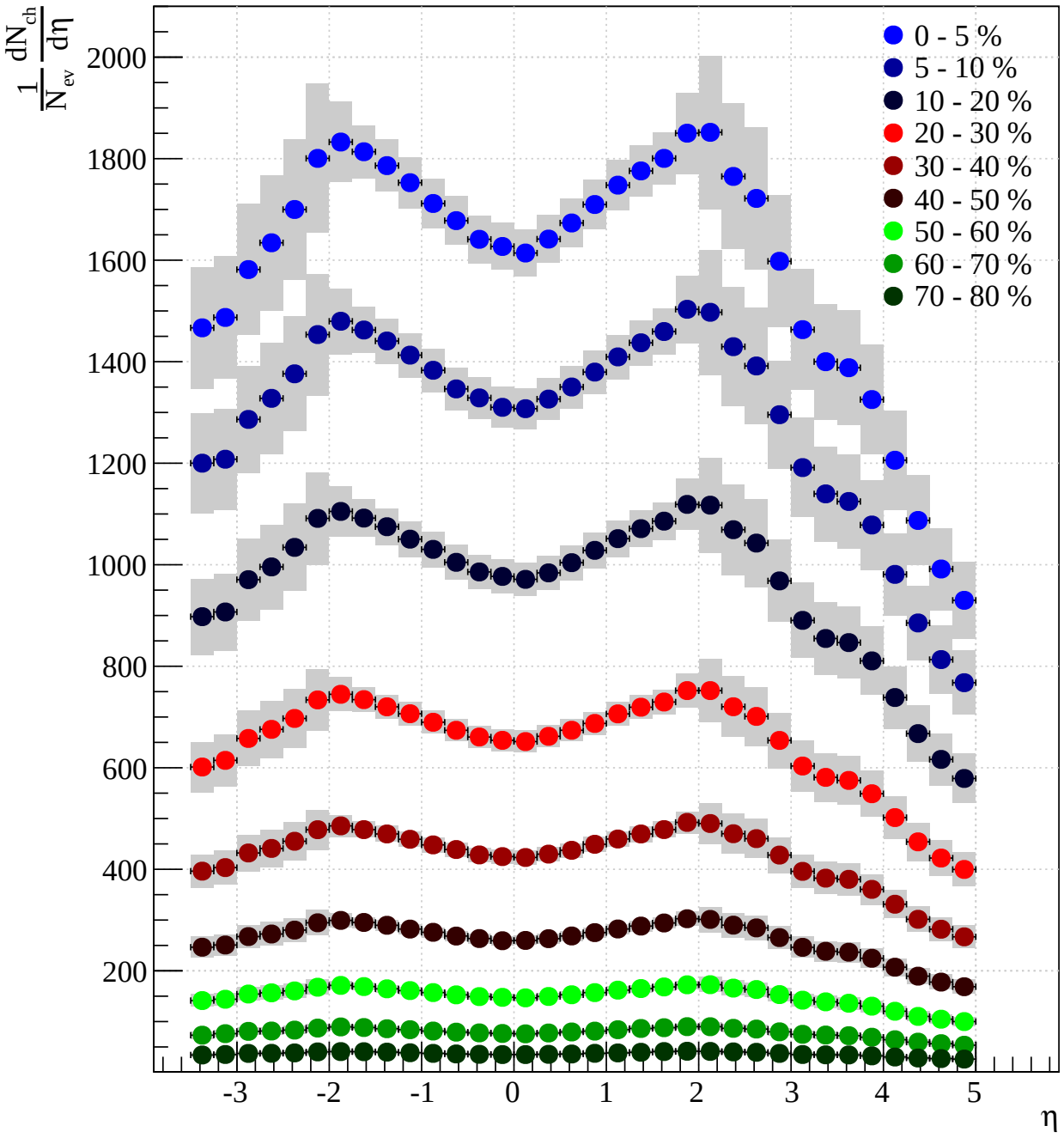

Figure 4: $\frac{1}{N}\frac{dN_{\mathrm{ch}}}{d\eta}$ for Pb+Pb for Minimum Bias events at $\sqrt{s_{NN}} = 2.76\,\mathrm{TeV}$ $-10\,\mathrm{cm} \leq v_z \leq 10\,\mathrm{cm}$, rebinned by a factor 5 in 10 centrality intervals [6].

7 Analysis for QM 2012 and Paper

7.1 Analysis

Following the development of the displaced vertex technique for VZERO [3] it was decided also to attempt such an analysis with the FMD using exactly the same event selection and centrality selection as the VZERO analysis.

The analysis described in this note was used successfully on these special events. Three detectors contribute to this measurement: SPD with tracklets covering $-2 < \eta < 2$ [7, 8], VZERO covering $-3 < \eta < -1.25$ and $1.25 < \eta < 5.25$, and FMD covering $-5 < \eta < -1.25$ and $1.25 < \eta < 5.5$. The extended coverage of the VZERO and FMD comes from the positions of the displaced vertices. The full pseudorapidity coverage of the combined measurement is $-5 < \eta < 5.5$.

To combine the measurements the individual measurements were weighted by their systematic error before a weighted average was taken to form the final $\frac{1}{N}\frac{dN_{\mathrm{ch}}}{d\eta}$. The systematic error is calculated as an average in quadrature with a contribution from the residual difference between the measurements.

Due to the nature of the ZDCvsZEM centrality determination (see [3] for details) the centrality selection of the measurement with SPD, VZERO, and FMD is limited to 30% central collisions. The centrality bins considered are thus $0-5\%$, $5-10\%$, $10-20\%$, and $20-30\%$.

The selected vertices with full pseudorapidity coverage for FMD in this analysis are 112.5 cm, 150 cm, 187.5 cm, 225 cm, 262.5 cm, 300 cm. For vertices $v_z > 300$ cm and $v_z < 112.5$ cm a cut is imposed in pseudorapidity to only accept data with $|\eta| > 4$ to avoid regions in ALICE known to have issues with the material budget description.

7.2 Analysis Performance

This section includes some plots to assess the validity of the analysis. This includes comparisons between the measurements used (SPD, VZERO, and FMD) and $\frac{1}{N}\frac{dN_{\mathrm{ch}}}{d\varphi}$ from the FMD.

Figure 5 shows the pseudorapidity coverage of the FMD when using FMD1 and FMD2I as a function of vertex with displaced vertices.

Figure 6 shows the results of the measurements of the SPD, VZERO, and FMD. It is seen that there is good agreement between the three different measurements albeit residual differences of up to 6% remain.

Figure 7 shows the ratios of the measurements of FMD and VZERO to the combined measurement and to the SPD measurement. It is seen that the residual differences are small and there is good agreement between the three different measurements.

Since $\frac{1}{N}\frac{dN_{\mathrm{ch}}}{d\eta}$ is an average taken over φ it is instructive to consider $\frac{1}{N}\frac{dN_{\mathrm{ch}}}{d\varphi}$ to check that these distributions are flat as they should be. Figure 8 shows examples of the $\frac{1}{N}\frac{dN_{\mathrm{ch}}}{d\varphi}$ distributions for FMD1. Figure 9 shows examples from FMD2 (inner ring). The two low points at $\varphi \sim 5.5$ in Figure 9 are understood as coming from two dying chips in FMD2I. They are considered dead in the final analysis and corrected for. It is seen that the trends are quite flat within $\sim 5\%$ as expected. The same trend is observed for all the distributions. Figure 10 shows the analysis performed for each vertex. The material budget effects for vertices < 112.5 cm are clearly seen. Figure 11 shows the ratio of the postive and negative pseudorapidities for the FMD. It is seen that there are discrepancies of up to $\sim 5\%$.

7.3 Results

This section summarizes the final results of the analysis and includes the figures for approval.

Figure 12 shows the combined $\frac{1}{N}\frac{dN_{\mathrm{ch}}}{d\eta}$ from SPD, VZERO, and FMD in the full pseudorapidity range of $-5 < \eta < 5.5$.

Figure 13 shows $dN/d\eta/(N_{part}/2)$ based on figure 12 and data taken from [8]. Using figure 13, figure 14 is

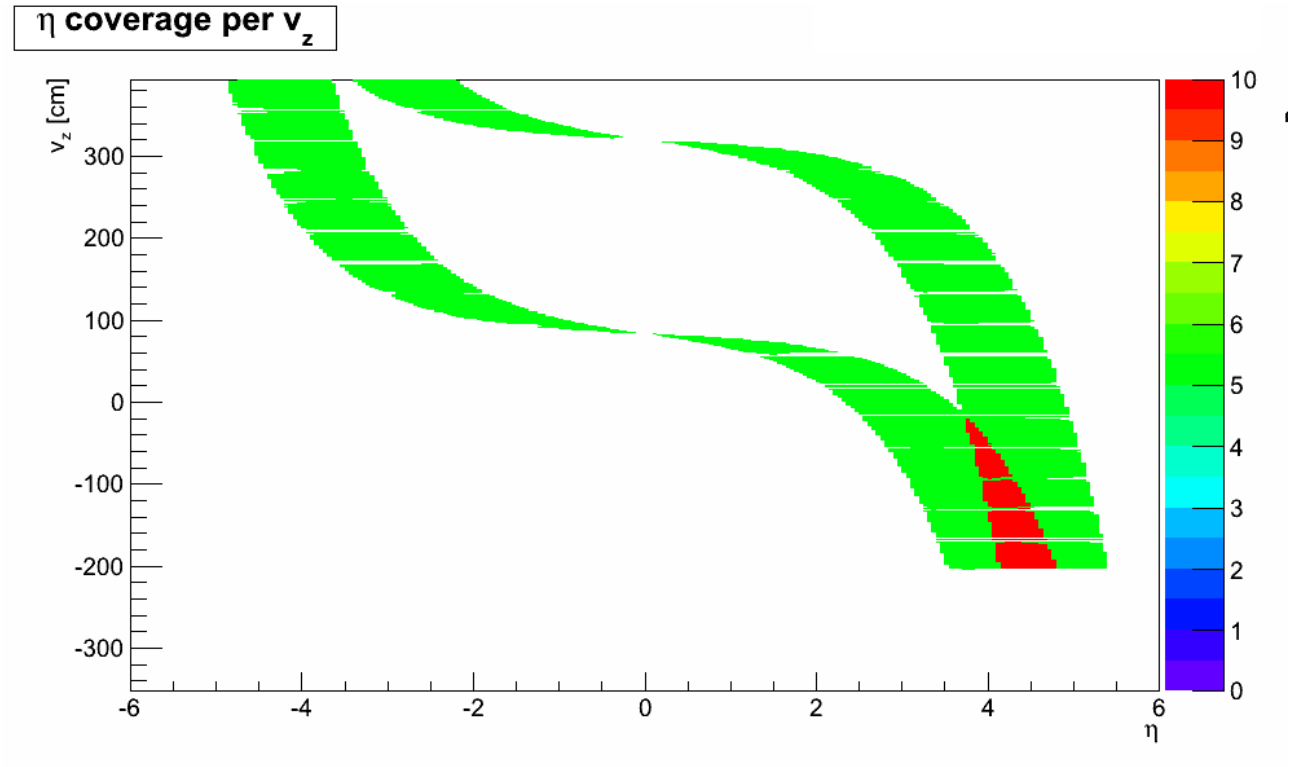

Figure 5: Pseudorapidity coverage of the FMD as a function of vertex with displaced vertices.

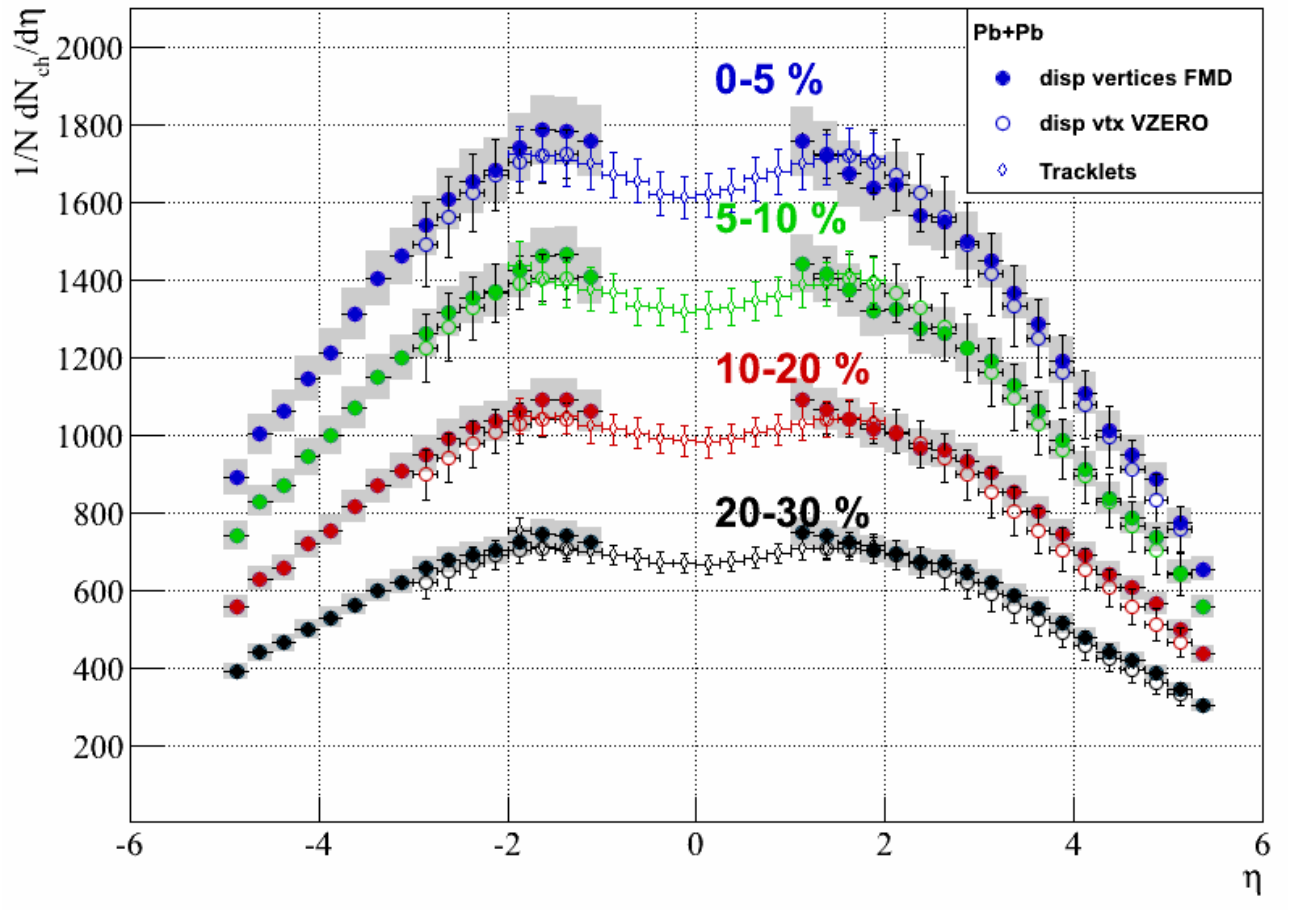

Figure 6: $\frac{1}{N}\frac{dN_{\mathrm{ch}}}{d\eta}$ measured with nominal vertices with the SPD and displaced vertices with VZERO and FMD. It is seen that there is good agreement between the measurements.

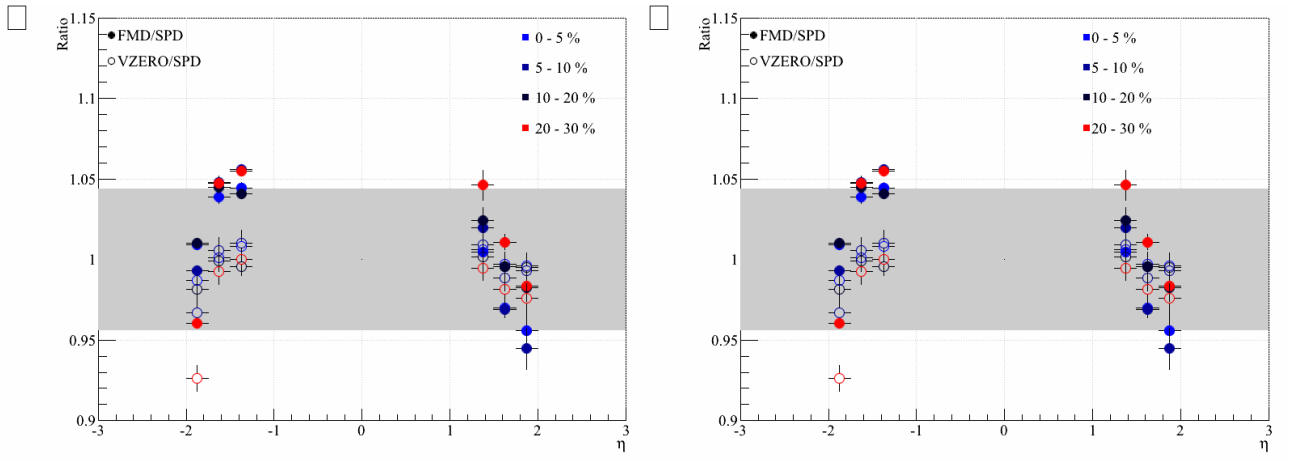

Figure 7: Left: Ratio of FMD and VZERO measurements to the combined $\frac{1}{N}\frac{dN_{\mathrm{ch}}}{d\eta}$ measured with SPD, VZERO and FMD. Right: Ratios of FMD and VZERO measurement to SPD measurement in regions of overlap. It is worth pointing out that the residual differences can come from the fact that the VZERO analysis uses SPD for absolute calibration while the FMD analysis does not. This means that the centrality determination for displaced vertices will affect the FMD analysis the most because the VZERO analysis has an additional constraint from the SPD analysis that uses the ZDCvsZEM centrality at midrapidity where it can be crosschecked with other means of centrality determination. Such a crosscheck is not possible elsewhere.

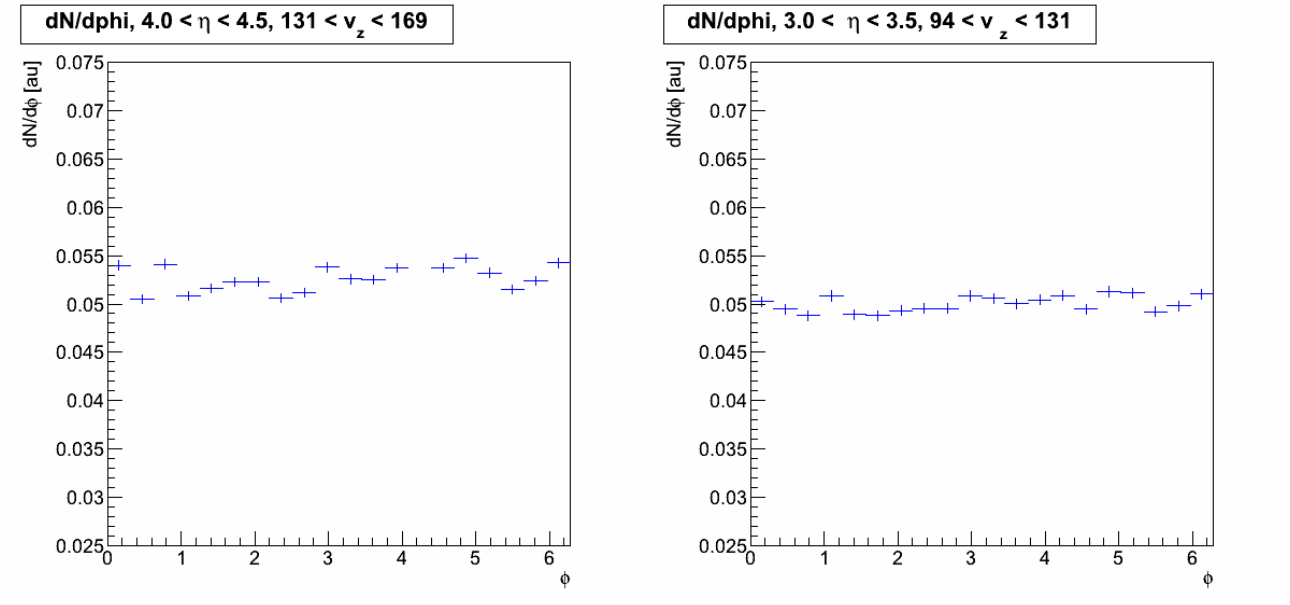

Figure 8: Examples of $\frac{1}{N}\frac{dN_{\mathrm{ch}}}{d\varphi}$ from FMD1 (positive pseudorapidities). The distributions are essentially flat.

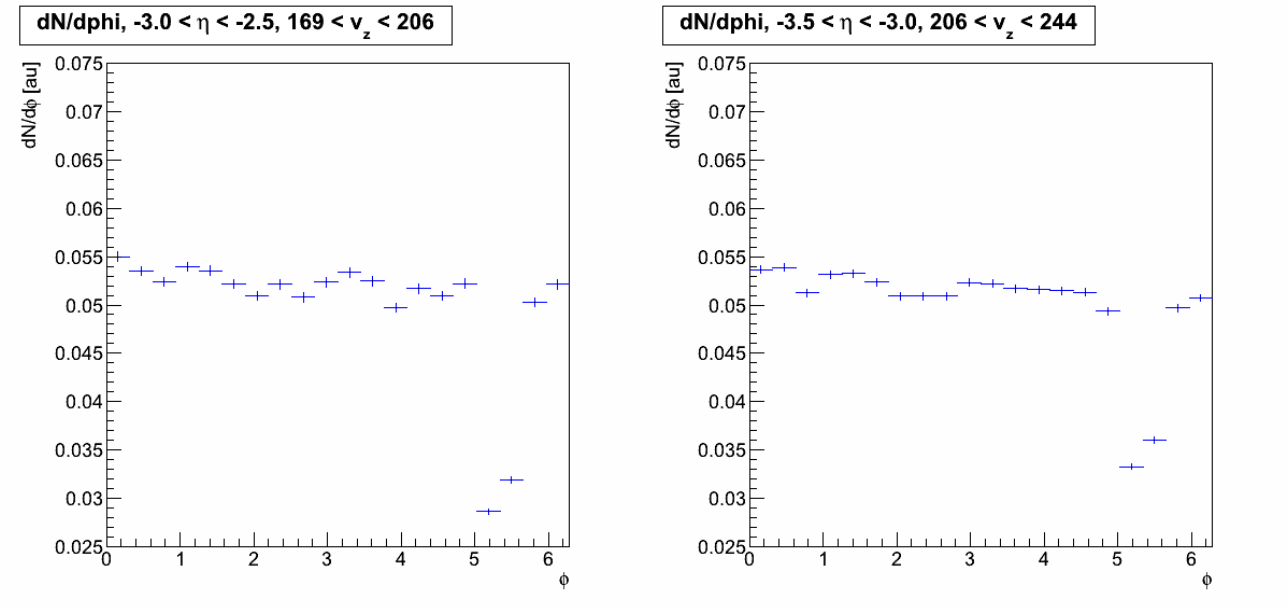

Figure 9: Examples of $\frac{1}{N}\frac{dN_{\mathrm{ch}}}{d\varphi}$ from FMD2I (negative pseudorapidities). The two low points at $\varphi \sim 5.5$ are understood as the result of two dying chips in FMD2I. They are considered dead in the final analysis and corrected for accordingly. Apart from these points, the distributions are essentially flat.

constructed. It shows the ratios of $dN/d\eta/(N_{part}/2)$ in the following η bins: $0.5 < \eta < 1.5$, $1.5 < \eta < 2.5$, $2.5 < \eta < 3.5$, $3.5 < \eta < 4.5$, and $4.5 < \eta < 5.5$ to the published $dN/d\eta/(N_{part}/2)$ at $-0.5 < \eta < 0.5$. These ratios are found to be flat for all pseudorapidity intervals. With the analysis presented in figure 12 it is also possible to study longitudinal scaling from LHC to RHIC energies. Figure 15 shows $\frac{1}{N}\frac{dN_{\mathrm{ch}}}{d\eta}$ as a function of $y' = \eta - y_{beam}$ from Figure 12 and results from the BRAHMS[9] and PHOBOS[10] experiments at RHIC. From the figure it is seen that with the wide coverage of the SPD, VZERO, and FMD measurement it is indeed likely that longitudinal scaling exist from RHIC to LHC energies. Finally the total number of produced charged particles, $N_{ch} = \int_{-y_{beam}}^{y_{beam}} \frac{1}{N}\frac{dN_{\mathrm{ch}}}{d\eta} d\eta$, has been calculated from the fits in Figure 12. The obtained values of N_{ch} versus N_{part} are shown in figure 16. The systematic errors on N_{ch} have been assessed by the procedure of varying fit functions discussed in [3].

7.4 Comparison to old Preliminary

At QM 2011 figures were approved for preliminary status and shown. Roughly six months later it was found that the execution of the FMD analysis had a flaw[8] which caused the results to be lower than what they should be. The top panel of Figure 17 shows a comparison between the distribution in Figure 12 and the preliminary (ALI-PREL-2536) shown at QM 2011. The top panel shows the same comparison with the proper FMD distribution instead of the incorrect one. It is clear that the agreement observed between VZERO, SPD, and FMD at QM 2011 does not hold with the FMD analysis run properly for nominal vertices.

7.5 Summary of Systematic Errors

Table 3 shows the various sources of systematic errors for the combined measurement of VZERO, SPD, and FMD collected from Table 4, [3], and [7, 8]. The 'common' section of the table refers to source of systematic errors identified as common in the different measurements. These errors were evaluated for the displaced vertices analysis in the following way:

- Centrality errors come from variation in the parameters used in the scaling of the ZEM signal (see [3]).

[8] A boolean variable was wrong in a configuration macro for FMD.

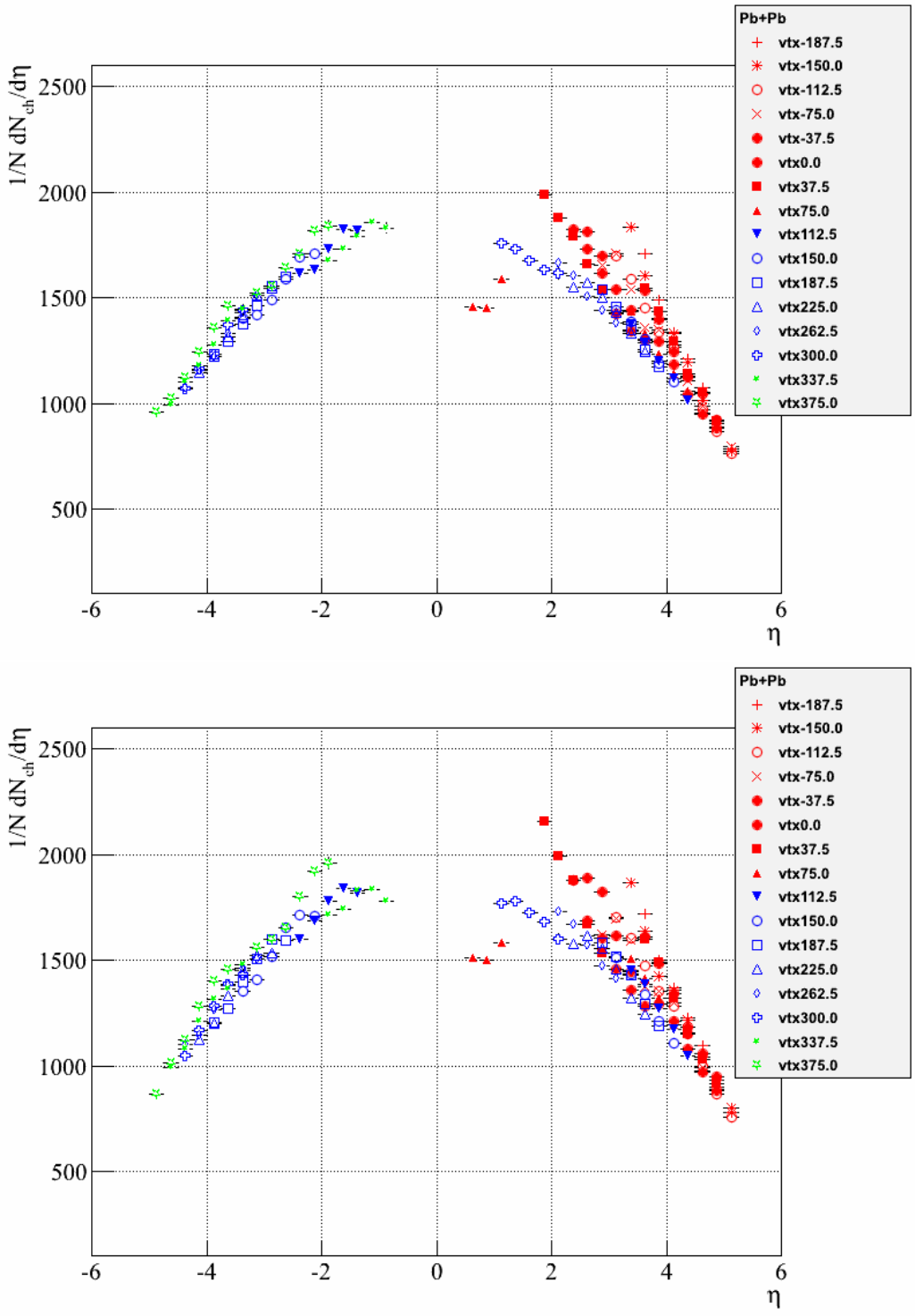

Figure 10: Top: Analysis per vertex for negative field data. Bottom: Analysis per vertex for positive field data. In the two plots the vertices where the full coverage is used are shown in blue. For the red and green points there a cut is applied for the pseudorapidity so that only points with $|\eta| > 4$ are used in the analysis.

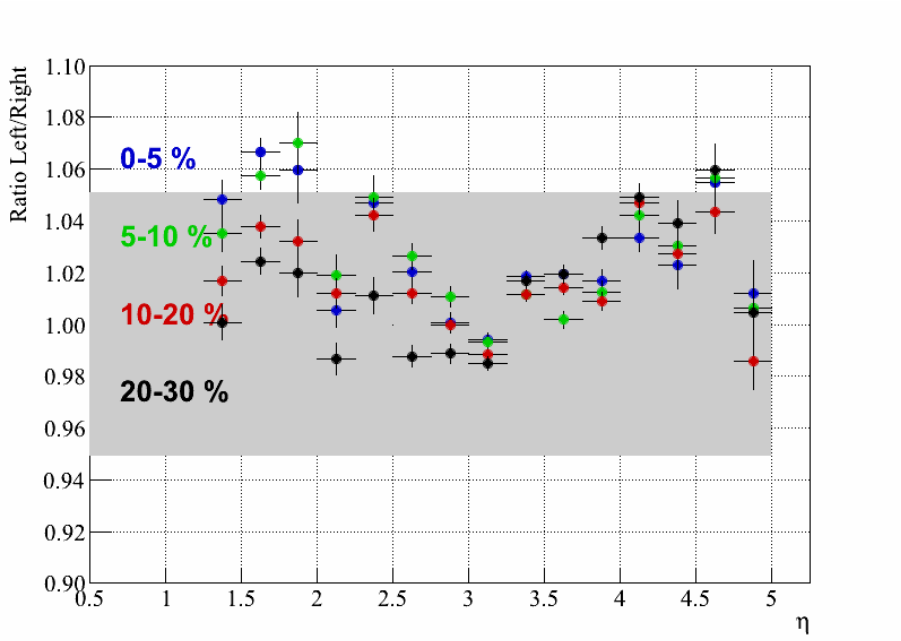

Figure 11: Ratios of the positive and negative pseudorapidities for the FMD (ratio is negative over positive). The grey band indicates the combined systematic error for FMD1I and FMD2I assuming excluding all contributions from event selection and material budget (i.e. the minimum systematic error between FMD1I and FMD2I).

- Material budget errors were estimated by analyzing a simulation and adding a weight of 0.9 or 1.1 to all physical processes except decays for all secondary particles. This approach was used in the absence of suitable ALICE simulation productions.
- p_T weights were developed to assess the effect of the difference in p_T spectra measured by ALICE and in the HIJING generator.

The errors are obtained using variation of the quantities studied in MC simulations. In particular the studies of the dependence on the material budget are carried out with special MC simulations where the material density of ALICE is increased.

7.6 Technical Details

Here, the technical aspects of the analysis are described. The SPD analysis was done on run 137366, reconstruction pass 2 while the FMD and VZERO analysis were carried out on a total of 126 runs (46 with negative field and 80 with positive field) to obtain the necessary statistics for the displaced vertices. These runs were selected to be of good quality for VZERO, SPD, FMD, and ZDC. These data were also from pass 2 reconstruction.

The AliRoot version for SPD is: **v5-03-24-AN**, for VZERO: **v5-03-28-AN**, and for FMD: **v5-03-26-AN**.

For the analysis of the displaced vertices presented here the production LHC12c2 was used (the simulation was done with an anchor run for each field polarity). This production includes the latest version (as of July 2012) of the ALICE geometry and alignment.

There is a twiki page for the paper using this analysis: `https://twiki.cern.ch/twiki/bin/viewauth/ALICE/PWGLFGeoPbPbdNdeta`.

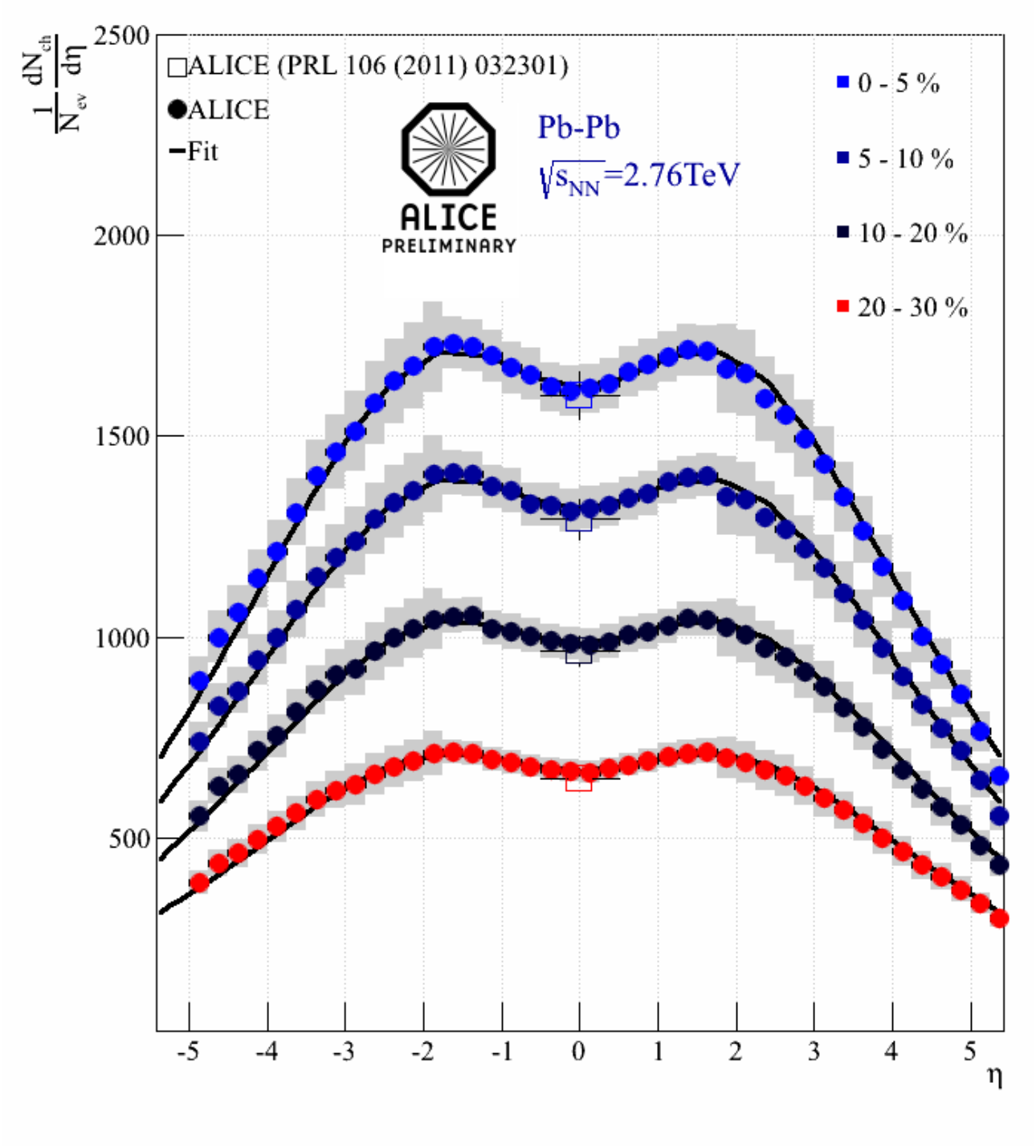

Figure 12: Request for ALICE preliminary: Combined $\frac{1}{N}\frac{dN_{\rm ch}}{d\eta}$ measured with SPD, VZERO and FMD. The VZERO and FMD measurements are made with displaced vertices and the SPD measurement is made at the nominal vertex. The fits are fits to a function $f(\eta) = A\exp(\frac{\eta-a_1}{2a_2^2}) - B\exp(\frac{\eta-b_1}{2b_2^2})$ i.e. a Gaussian centered on $\eta = 0$ subtracted from a similar Gaussian.

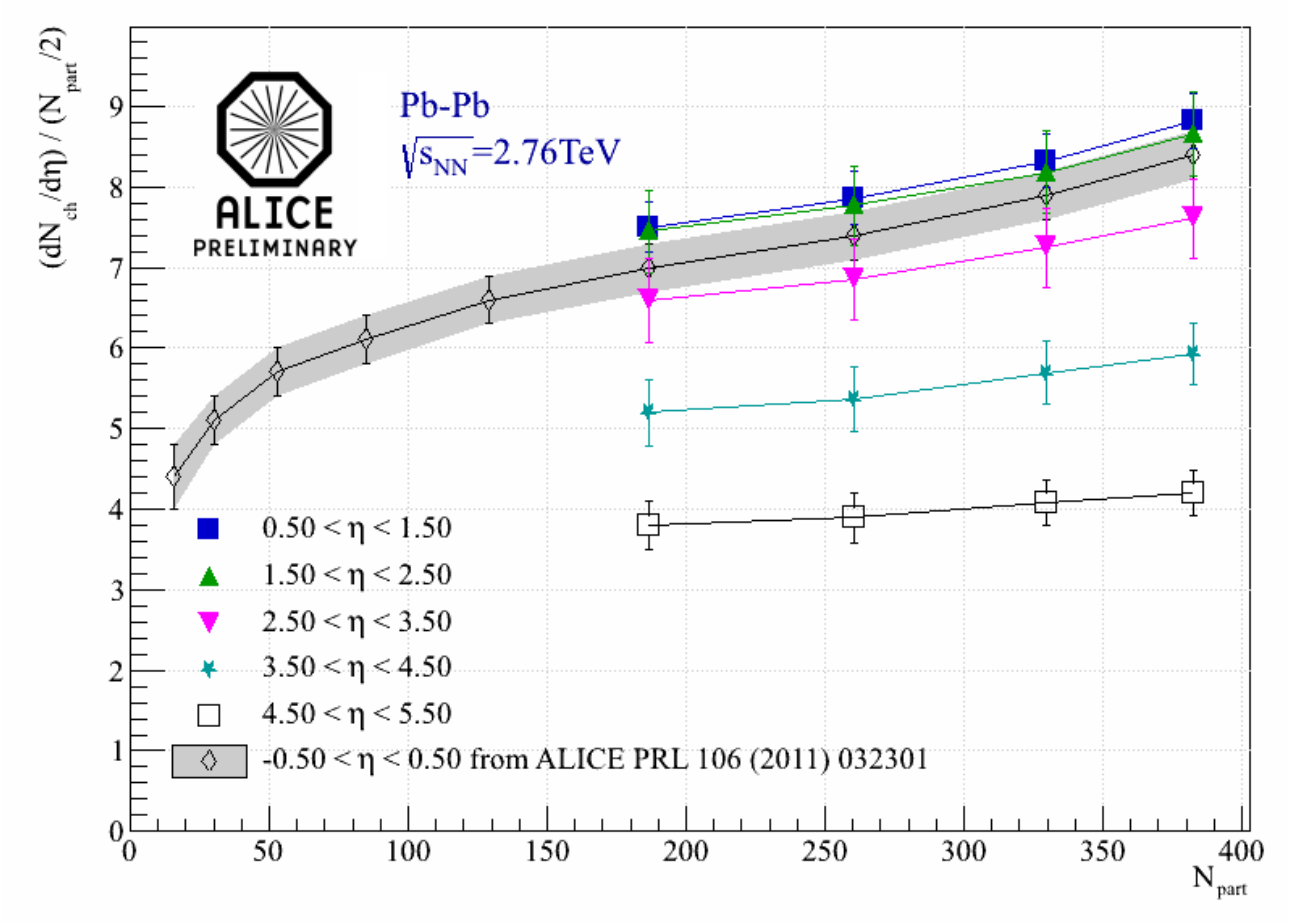

Figure 13: Request for ALICE preliminary: The $dN/d\eta/(N_{part}/2)$ measured with SPD, VZERO and FMD. The VZERO and FMD measurements are made with displaced vertices and the SPD measurement is made at the nominal vertex. The values of N_{part} and the measurement at $-0.5 < \eta < 0.5$ taken from [8].

Source of Error	Magnitude
Common	
Centrality	1-4%
p_T weights (FMD+VZERO)	2%
Material budget(FMD+VZERO)	4%
Generator	2%
SPD	
Background Subtraction	0.1%-2%
Particle Mix	1%
Weak Decays	1 %
Extrapolation to zero p	2%
VZERO	
Fluctuation between rings	3%
Normalization	3%-4%
FMD	
Variation of Cuts	2%
Calculation of Multiplicity	3%

Table 3: The table summarizes the systematic errors in the SPD[7, 8], VZERO[3], and FMD[6].

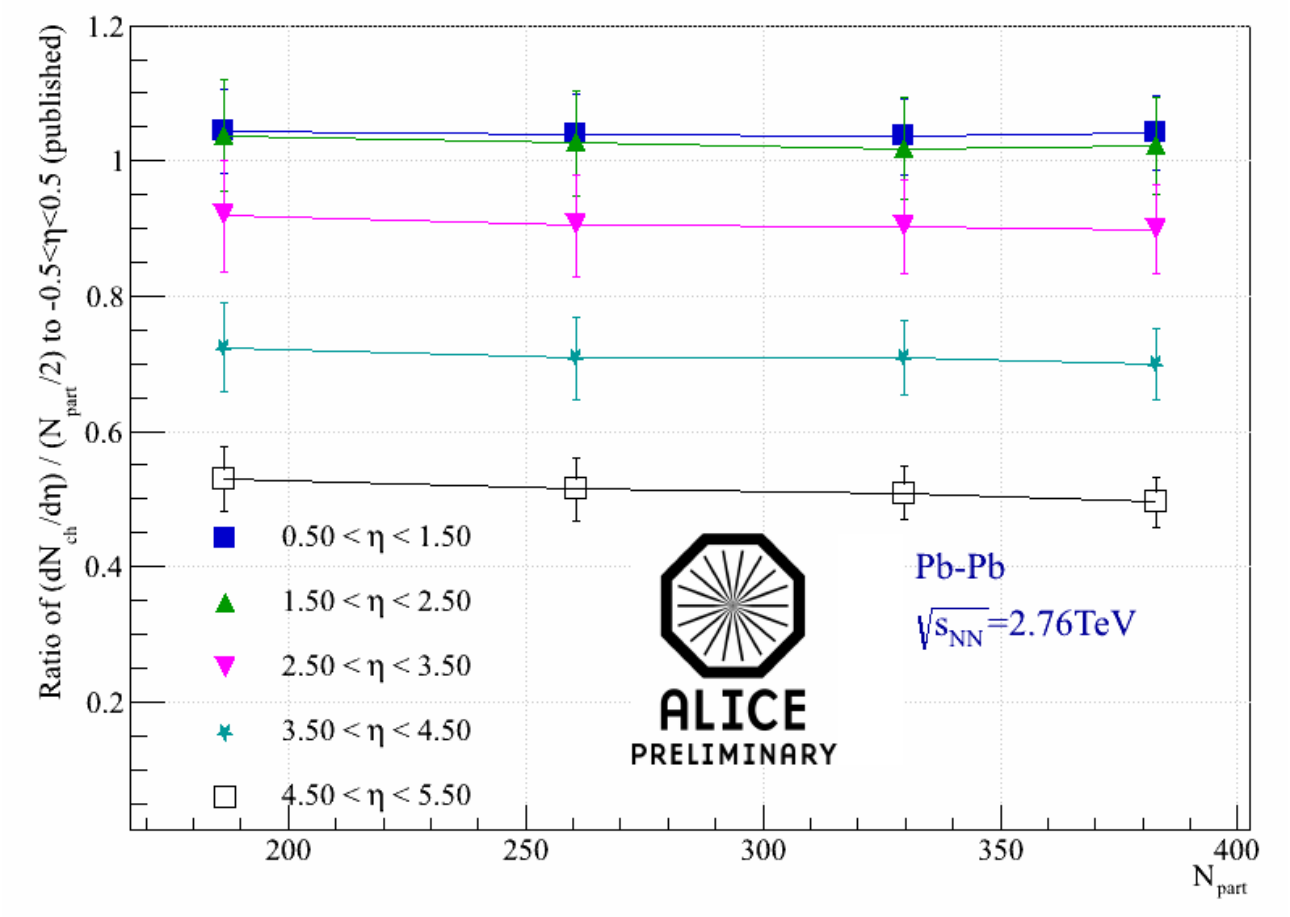

Figure 14: Request for ALICE preliminary: Ratios of $dN/d\eta/(N_{part}/2)$ at $0.5 < \eta < 1.5$, $1.5 < \eta < 2.5$, $2.5 < \eta < 3.5$, $3.5 < \eta < 4.5$, and $4.5 < \eta < 5.5$ to the published $dN/d\eta/(N_{part}/2)$ at $-0.5 < \eta < 0.5$. The ratios are found to be flat for all the pseudorapidity intervals.

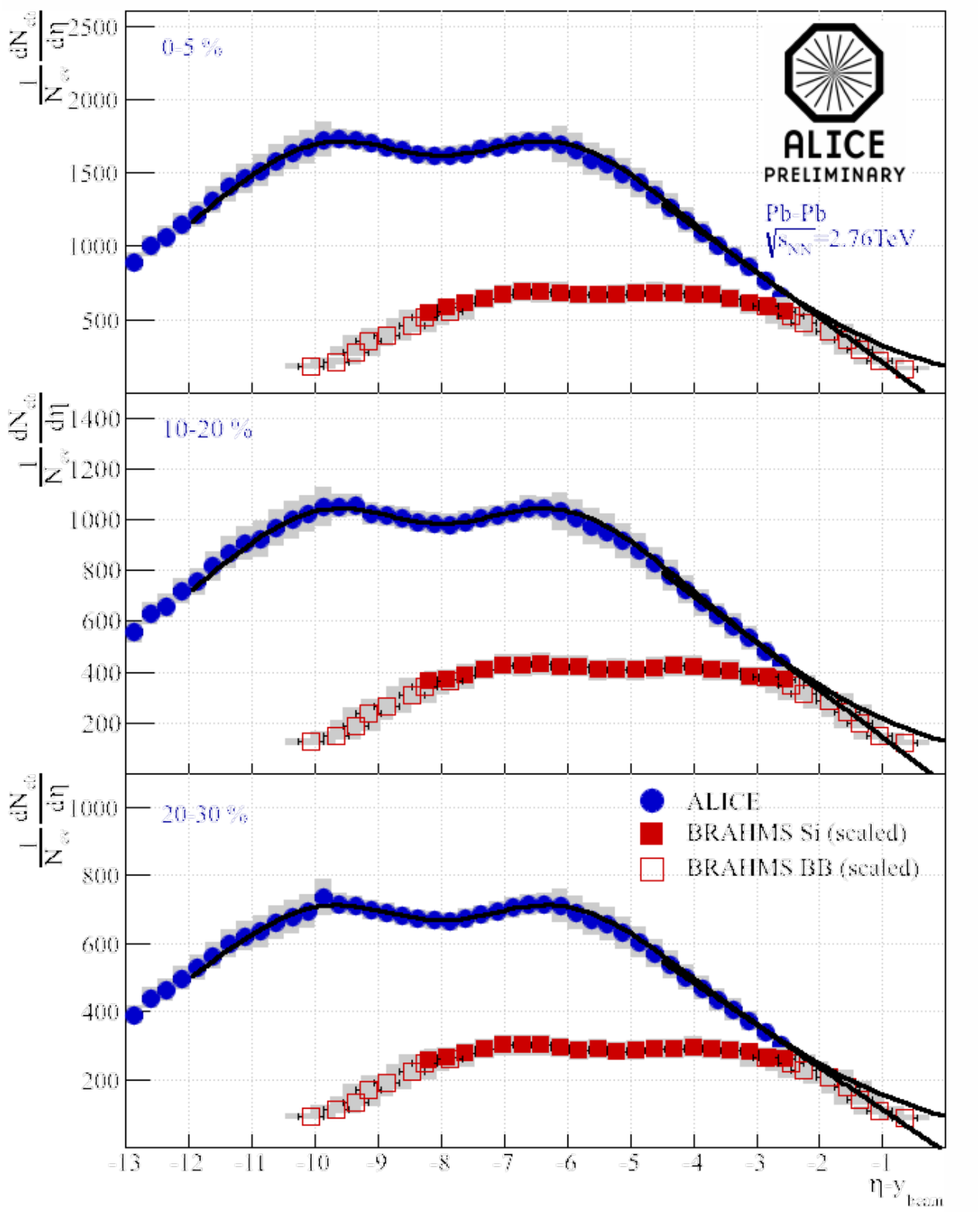

Figure 15: Request for ALICE preliminary: Study of Longitudinal scaling. $\frac{1}{N}\frac{dN_{\mathrm{ch}}}{d\eta}$ as a function of $y' = \eta - y_{beam}$ from Figure 12 and the BRAHMS[9] and PHOBOS[10] experiments at RHIC. The fits are the function from figure 12 and a straight line ending in $\eta = y_{beam}$. From the figure it seems likely that longitudinal scaling exists from RHIC to LHC energies.

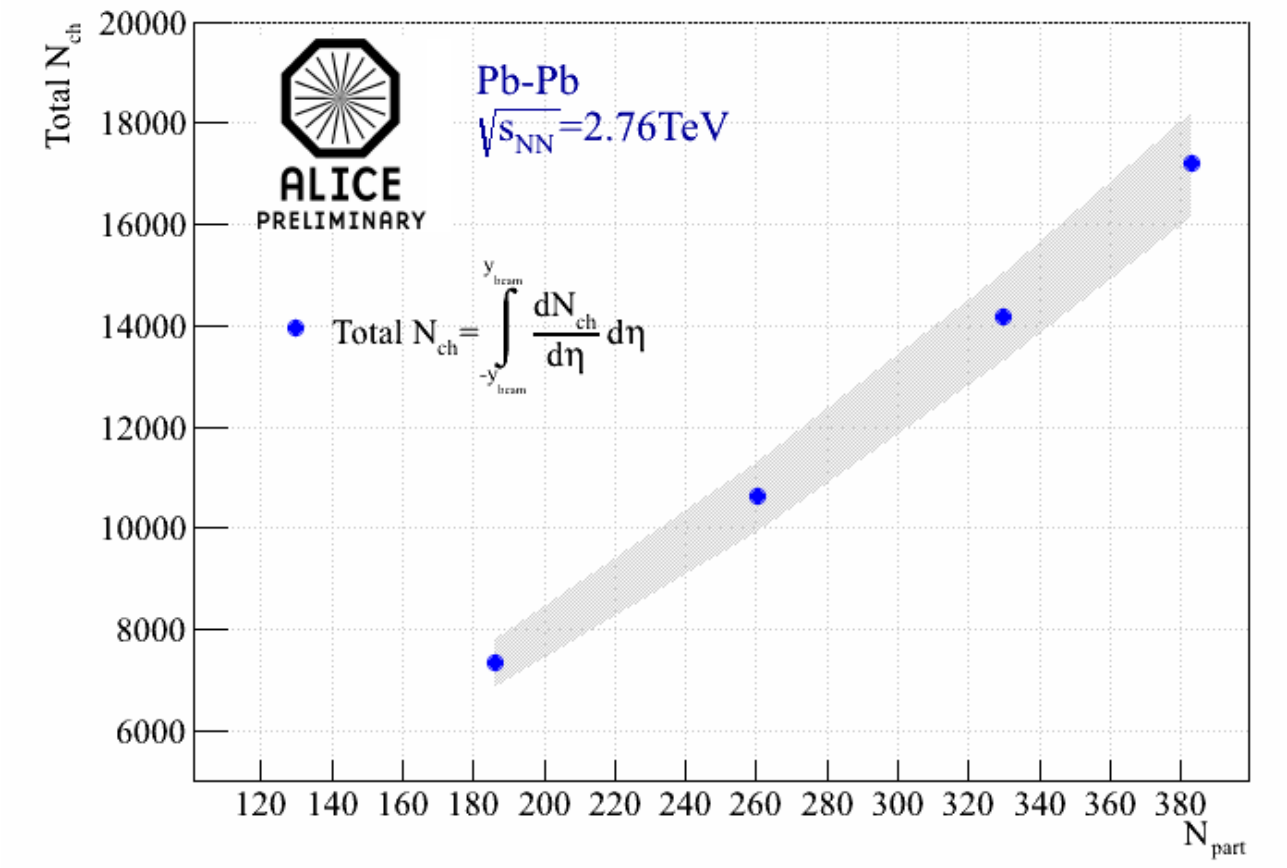

Figure 16: Request for ALICE preliminary: Total number of charged particles, $N_{ch} = \int_{-y_{beam}}^{y_{beam}} \frac{1}{N} \frac{dN_{ch}}{d\eta} d\eta$, obtained from the fitted function in figure 12. The systematic errors on this plot were assessed by variation of the fit function as described in [3].

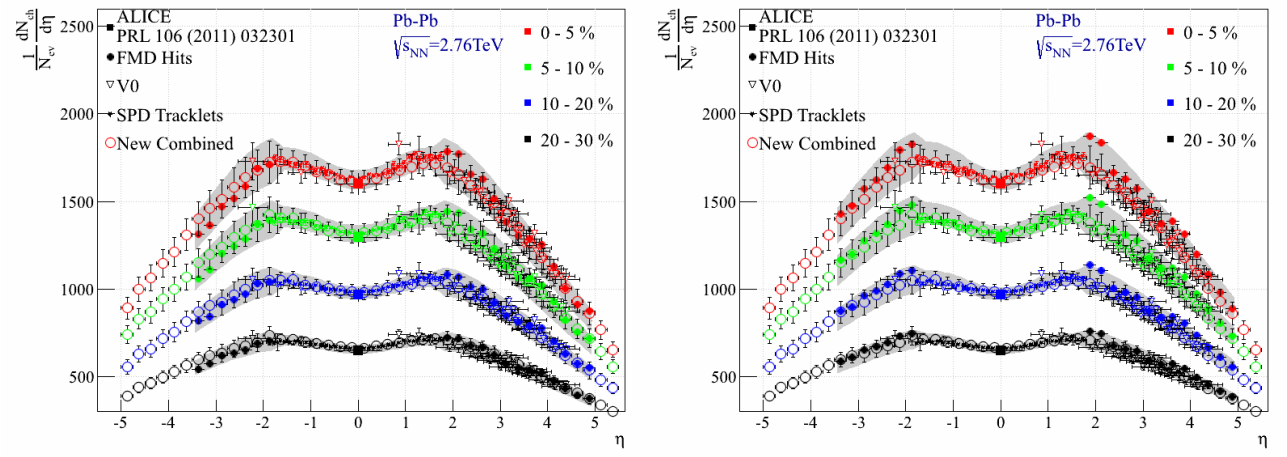

Figure 17: Left: Comparison of new combined $\frac{1}{N} \frac{dN_{ch}}{d\eta}$ to the data shown at QM 2011. Right: The same comparison with the properly run FMD analysis at nominal vertices ('FMD Hits'). The difference is clearly seen around $|\eta| \sim 2$.

A Nomenclature

Symbol	Description
INEL	In–elastic event
INEL > 0	In–elastic event with at least one tracklet in the SPD in the region $-1 \leq \eta \leq 1$
NSD	Non–single–diffractive event. Single diffractive events are events where one of the incident collision systems (proton or nucleus) is excited and radiates particles, but there is no other processes taking place
N_{T}	Number of events with a valid trigger
N_{V}	Number of events with a valid trigger *and* a valid vertex.
N_{A}	Number of events with a valid trigger *and* a valid vertex *within* the selected vertex range.
$N_{a,c,ac,e}$	Number of events with background triggers *A*, *B*, *AC*, or *E*, *and* a valid off-line trigger of the considered type. Background triggers are typically flagged with the trigger words `CINT1-A`, `CINT1-C`, `CINT1-AC`, `CINT1-E`, or similar.
N_{ch}	Charged particle multiplicity
$N_{\mathrm{ch,primary}}$	Primary charged particle multiplicity as given by simulations
$N_{\mathrm{ch,FMD}}$	Number of charged particles that hit the FMD as given by simulations
$N_{\mathrm{ch},t}$	Number of charged particles in an FMD strip as given by evaluating the energy response functions F
F	Energy response function (see (2))
Δ_{mp}	Most probably energy loss
ξ	'Width' parameter of a Landau distribution
σ	Variance of a Gaussian distribution
a_i	Relative weight of the *i*–fold MIP peak in the energy loss spectra.
A_t^{φ}	Azimuthal acceptance of strip t
$S_v(\eta,\varphi)$	Secondary particle correction factor in (η,φ) for a given vertex bin v
$A_{v,i}^{\eta}(\eta,\varphi)$	Acceptance in (η,φ) for a given vertex bin v
$\left.\frac{d^2N_{\mathrm{ch}}}{d\eta\,d\varphi}\right\vert_{incl,r,v,i}$	Inclusive (primary *and* secondary) charge particle density in event i with vertex v, for FMD ring r.
$\left.\frac{d^2N_{\mathrm{ch}}}{d\eta\,d\varphi}\right\vert_{r,v,i}$	Primary charged particle density in event i with vertex v for FMD ring r.
$\left.\frac{d^2N_{\mathrm{ch}}}{d\eta\,d\varphi}\right\vert_{v,i}$	Primary charged particle density in event i with vertex v
$I_{v,i}(\eta)$	η acceptance of event i with vertex v
$I(\eta)$	Integrated η acceptance over N_{A} events. Note, that this has a value of N_{A} for (η) bins where we have full coverage
X_t	Value X for strip number t (0-511 for inner rings, 0-255 for outer rings)
X_r	Value X for ring r (where rings are FMD1i, FMD2i, FMD2o, FMD3o, and FMD3i in decreasing η coverage).
X_v	Value X for vertex bin v (typically 10 bins from -10cm to +10cm)
X_i	Value X for event i

Table 4: Nomenclature used in this document

B Second pass example code

```
void Analyse(int mask=AliAODForwardMult::kInel,
             float vzLow=-10, float vzHigh=10, float trigEff=1)
{
  gSystem->Load("libANALYSIS.so");       // Load analysis libraries
  gSystem->Load("libANALYSISalice.so"); // General ALICE stuff
  gSystem->Load("libPWGLFforward2.so");  // Forward analysis code

  int                 nT      = 0;              // # of ev. w/trigger
  int                 nV      = 0;              // # of ev. w/trigger&vertex
  int                 nA      = 0;              // # of accepted ev.
  int                 nBg     = 0;              // # of background ev
  TH2D*               sum     = 0;              // Summed hist
  AliAODForwardMult* mult     = 0;              // AOD object
  TFile*              file    = TFile::Open("AliAODs.root","READ");
  TTree*              tree    = static_cast<TTree*>(file->Get("aodTree"));
  tree->SetBranchAddress("Forward", &forward); // Set the address

  for (int i = 0; i < tree->GetEntries(); i++) {
    // Read the i'th event
    tree->GetEntry(i);

    // Create sum histogram on first event - to match binning to input
    if (!sum)
      sum = static_cast<TH2D*>(mult->GetHistogram()->Clone("d2ndetadphi"));

    // Calculate beta=A+C-E
    if (mult->IsTriggerBits(mask|AliAODForwardMult::kA))    nBg++;
    if (mult->IsTriggerBits(mask|AliAODForwardMult::kC))    nBg++;
    if (mult->IsTriggerBits(mask|AliAODForwardMult::kE))    nBg--;

    // Other trigger/event requirements could be defined
    if (!mult->IsTriggerBits(mask)) continue;
    nT++;

    // Check if we have vertex and select vertex range (in centimeters)
    if (!mult->HasIpZ()) continue;
    nV++;

    if (!mult->InRange(vzLow, vzHigh) continue;
    nA++;

    // Add contribution from this event
    sum->Add(&(mult->GetHistogram()));
  }

  // Get acceptance normalisation from underflow bins
  TH1D* norm    = sum->ProjectionX("norm", 0, 0, "");
  // Project onto eta axis - _ignoring_underflow_bins_!
  TH1D* dndeta = sum->ProjectionX("dndeta", 1, -1, "e");
  // Normalize to the acceptance, and scale by the vertex efficiency
  dndeta->Divide(norm);
  dndeta->Scale(trigEff * nT/nV / (1 - nBg/nT), "width");
  // And draw the result
  dndeta->Draw();
}
```

Listing 1: Example 2nd pass code to do $\frac{1}{N}\frac{dN_{\mathrm{ch}}}{d\eta}$

C ΔE fits

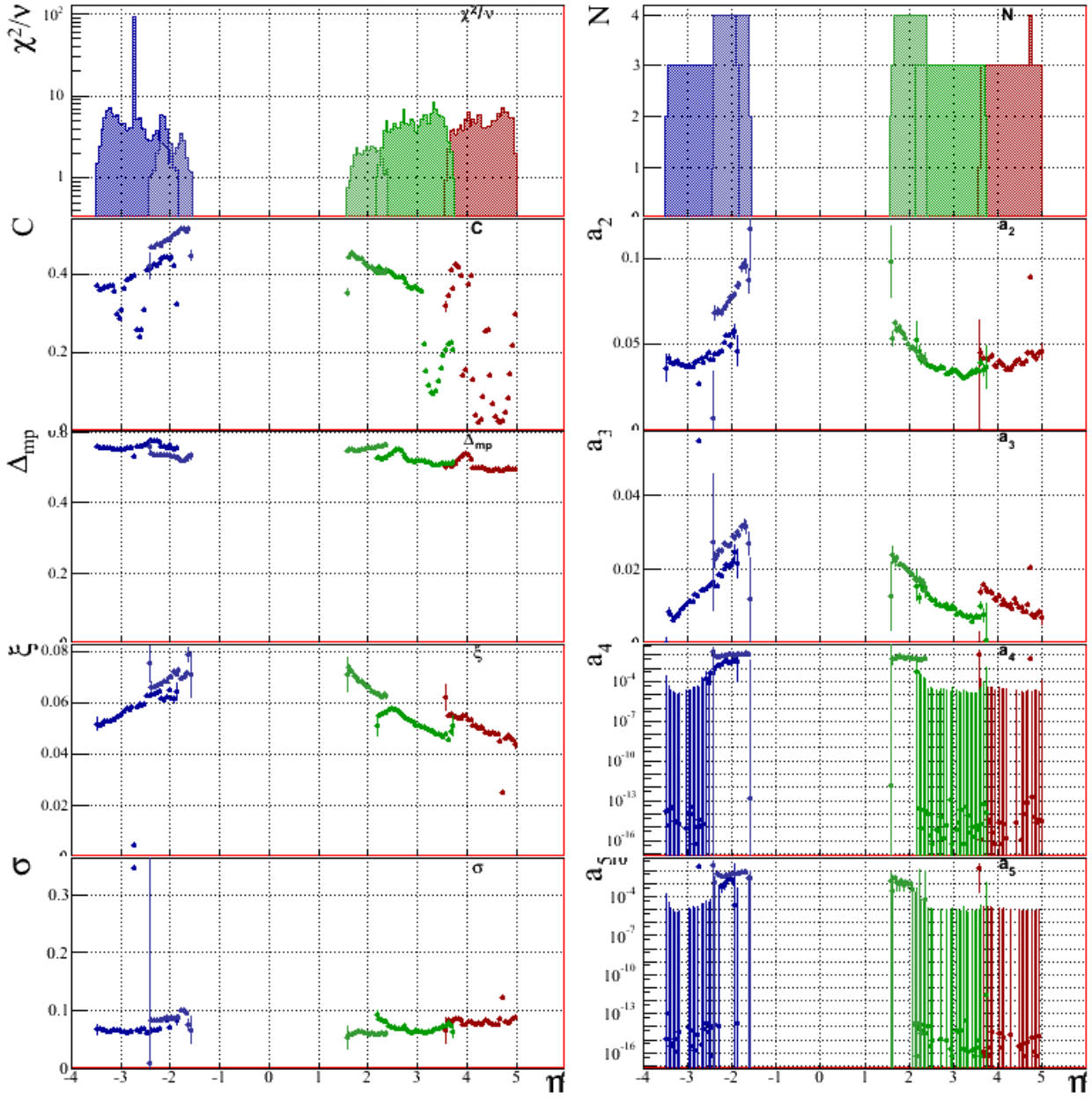

Figure 18: Summary of energy loss fits in each η bin (see also Section 2.3.1).
On the left side: Top panel shows the reduced χ^2, second from the top shows the found scaling constant, 3$^{\text{rd}}$ from the top is the most probable energy loss Δ_{mp}, 4$^{\text{th}}$ shows the width parameter ξ of the Landau, and the 5$^{\text{th}}$ is the Gaussian width σ. Δ_{mp}, ξ, and σ have units of $\Delta E/\Delta E_{mip}$.
On the right: The top panel shows the maximum number of multi–particle signals that where fitted, and the 4 bottom panels shows the weights a_2, a_3, a_4, and a_5 for 2, 3, 4, and 5 particle responses.

References

[1] ALICE Collaboration, Bearden, I. G. *et al ALICE technical design report on forward detectors: FMD, T0 and V0*, CERN, 2004, CERN-LHCC-2004-025

[2] Christensen, C. H., *The ALICE Forward Multiplicity Detector — From Design to Installation*, Ph.D. thesis, University of Copenhagen, 2009, http://www.nbi.dk/~cholm/.

[3] Guilbaud, M. *et al*, *Measurement of the charged-particle multiplicity density at forward rapidity with ALICE VZERO detector in central Pb-Pb collision at* $\sqrt{s_{NN}} = 2.76\,TeV$, ALICE internal note, 2012, https://aliceinfo.cern.ch/Notes/node/17/.

[4] S. Hancock, F. James, J. Movchet *et al.*, "Energy Loss Distributions For Single Particles And Several Particles In A Thin Silicon Absorber," Nucl. Instrum. Meth. **B1** (1984) 16, http://cdsweb.cern.ch/record/147286/files/cer-000058451.pdf.

[5] S. Hancock, F. James, J. Movchet *et al.*, "Energy Loss And Energy Straggling Of Protons And Pions In The Momentum Range 0.7-gev/c To 115-gev/c," Phys. Rev. **A28** (1983) 615, http://cdsweb.cern.ch/record/145395/files/PhysRevA.28.615.pdf.

[6] Dalsgaard, H. H., *Pseudorapidity Densities in p+p and Pb+Pb collisions at LHC measured with the ALICE experiment*, Ph.D. thesis, University of Copenhagen, 2011, http://www.nbi.dk/~canute/thesis.pdf.

[7] Shahoyan, R. *Determination of* $\frac{1}{N}\frac{dN_{ch}}{d\eta}$ *in Pb-Pb collision at 2.76 A TeV with SPD tracklets*, ALICE internal note 2012, https://aliceinfo.cern.ch/Notes/node/59/.

[8] K. Aamodt *et al.* [ALICE Collaboration], Phys. Rev. Lett. **106** (2011) 032301 [arXiv:1012.1657 [nucl-ex]].

[9] I. G. Bearden *et al.* [BRAHMS Collaboration], Phys. Rev. Lett. **88** (2002) 202301 [nucl-ex/0112001].

[10] B. Alver *et al.* [PHOBOS Collaboration], Phys. Rev. C **83** (2011) 024913 [arXiv:1011.1940 [nucl-ex]].